RESEARCH ARTICLE

Macromolecular Materials and Engineering

www.mame-journal.de

Multifunctional, Wash Durable and Re-usable Conductive Textiles for Wearable Electro/Physiological Monitoring

*Ravinder Reddy Kisannagar, Mukesh Singh, and Dipti Gupta**

Intelligent functionalities coupled textiles have received massive attention in the wearable health monitoring devices owing to their lightweight, ease of wearability, intrinsic flexibility, and comfortable texture. This article describes multifunctional, highly conductive, wash durable, and re-usable reduced graphene oxide (RGO) coated polyester knitted textiles by a simple, cost effective, and scalable dip-dry-reduce approach and a novel approach to integrate as fabricated RGO coated polyester knitted textile (RGT) with the wearable elastic band for electro/physiological signal monitoring. The RGT exhibits high conductivity of 0.23 KΩ sq^{-1} and excellent wash durability. The RGT textile as a strain sensor shows a high sensitivity of 4.1 and 8 at a strain of 5% along the course and wale direction, respectively, stability and durability for more than 1500 cycles and also shows its excellent performance in human motion detection. Obtained electrophysiological signals from the RGT electrodes integrated wearable elastic band are comparable to those of the conventional Ag/AgCl electrodes. Owing to its comfortable texture, ease of wearability, stability, and wash durability, the RGT has potential applications in the future wearable electronic devices.

1. Introduction

The rapid development of electronic medical devices for health monitoring is evolving toward flexible and stretchable devices, grabbing the attention of several researchers and technologists owing to its ease of wearability and prolonged continuous monitoring without losing patient's comfort.[1–4] Flexible and wearable electronic devices have attracted huge attention because of their potential applications in soft robotics, human-machine interfaces, energy devices, sensor devices, and physiological signal monitoring.[5–10] Most of the flexible and wearable electronics devices have been fabricated by using conductive nanomaterials as active materials and flexible polymers as a substrate material.[11–13] Conductive nanomaterials include carbon nanotubes, graphene, metal nanowires and nanoparticles, and conductive polymers such as poly (3, 4-ethylenedioxythiophene)-poly (styrenesulfonate) (PDOT: PSS), polypyrrole and polyaniline, while flexible polymers include polydimethylsiloxane (PDMS), Eco-flex, natural rubber, and polyethylene terephthalate (PET).[14–21] However, flexible and wearable electronics prepared by conductive materials combined with the flexible polymers have some disadvantages as they are unbreathable, not comfortable for long-term wearing, and are difficult to integrate with daily clothing. In this context, conductive textiles have offered new technological platforms for developing flexible and wearable electronic devices.[22–27] In particular, strain/pressure sensors for physiological signal monitoring and dry electrodes for electrophysiological signal acquisition have found a wide scope of interest because of their lightweight, scalability, intrinsic flexibility, low cost, breathable nature, and facile incorporation to daily clothing.[28–34] Several research groups have employed carbon and its derivatives, metal nanomaterials, conductive polymers, and their hybrid materials to fabricate conductive textiles by various methods such as electroplating, vacuum deposition, printing, layer by layer assembly, and dip coating.[31,35–41] Textiles coated with metal nanomaterials exhibited high conductivity, however, it is challenging to obtain their uniform coating and adhesion with the textile.[41] The conductive polymer coated textiles provide low conductivity that limit their suitability for wearable electronics to some extent.[41] On the other hand, textile coated with carbon and its derivatives facilitates uniform coating as well as good adhesion with the textile owing to van der Waals interactions.[41,42] However, wash durability, reliability, and re-usability of conductive textiles and a novel method to integrate those conductive textiles with day to day clothings are essential for flexible and wearable electronic applications.

In this report, we made efforts to eliminate these issues, as faced by carbon nanomaterials coated textiles by using a facile, inexpensive, and scalable dip-dry-reduce method to coat multifunctional reduced graphene oxide (RGO) on a polyester knitted textile (RGT). The RGT shows high conductivity (0.23 KΩ sq^{-1}) and excellent wash durability. The RGT as a strain sensor reveals the sensitivity of 4.1 and 8 in the course and wale direction, respectively. The RGT strain sensor illustrates stability, durability for more than 1500 cycles, and outstanding performance in human motion detection. We employed a novel approach to integrate the RGT as flexible dry electrodes to the wearable elastic

R. R. Kisannagar, M. Singh, Prof. D. Gupta
Plastic Electronics and Energy lab (PEEL)
Department of Metallurgical Engineering and Materials Science
Indian Institute of Technology Bombay
Powai, Mumbai 400076, India
E-mail: diptig@iitb.ac.in

The ORCID identification number(s) for the author(s) of this article can be found under https://doi.org/10.1002/mame.202000804

DOI: 10.1002/mame.202000804

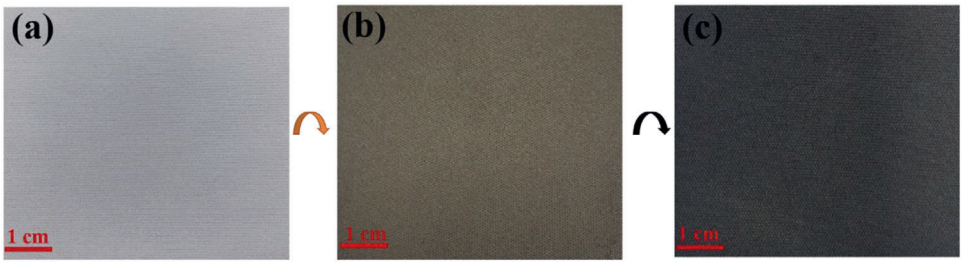

Figure 1. a) Pristine polyester knitted textile, b) graphene oxide (GO) coated polyester knitted textile, and c) reduced graphene oxide (RGO) coated polyester knitted textile (RGT).

band by using iron-on-adhesive followed by attaching snap buttons. The RGT electrodes integrated wearable elastic band could monitor the continuous and long-term electrophysiological signals. The signal to noise ratios (SNR) of electrocardiogram (ECG) signal acquired from the RGT electrodes is about 23.45 dB while the conventional Ag/AgCl electrodes are about 25 dB. Similar ECG signals were observed for every 3 h upon continuously wearing for 12 h, suggesting continuous and long-term monitoring of electrophysiological signals without any allergic effect. Due to its high conductivity, stability, and wash durability, the RGT electrodes integrated wearable elastic band can be used multiple times without losing signal quality.

2. Experimental Section

2.1. Materials

Graphite powder (<20um, synthetic, 99%), hydriodic acid (57 wt% in H_2O, distilled, stabilized, 99.95%), sodium bicarbonate (>99.5%) were purchased from Sigma Aldrich. Sodium nitrate (>99%), potassium permanganate (>99%), sulfuric acid (98%), hydrogen peroxide (30%), hydrochloric acid (37%), and acetic acid (100%) were obtained from MERCK and used as received. Pristine 100% polyester knitted textiles with a thickness of 400 µm, elastic band, iron-on adhesive, metal snaps and epoxy glue were purchased from the commercial sources.

2.2. GO Preparation

Graphene oxide (GO) was synthesized from Graphite powder using the modified Hummers and Offenman's method.[42]

2.3. Fabrication of Reduced Graphene Oxide (RGO) Coated Textile (RGT)

Figure 1a–c illustrates the fabrication process of RGO coated textile (RGT). As synthesized GO solution (1 mg mL^{-1}) was obtained in a crystallizing dish followed by sonication for 30 min. The textile used in the work is an interlocked knitted textile made of continuous polyester filament yarn. A course of the knit is the series of loops that intermesh in a vertical direction while wale of the knit is the interconnected loops in a horizontal direction, as shown in Figure S1 (Supporting Information).

As received polyester knitted textile was cut into 6 × 6 cm^2, washed with soap water followed by rinsing with DI water several times and then dried at room temperature in ambient condition as shown in Figure 1a. After that, the textile was soaked in GO solution for several hours and dried at 80 °C. Upon soaking the textile in GO solution, GO solution is absorbed into the textile due to capillary effect, and GO nanosheets are coated on the textile surface because of the interaction between the oxidized groups of the GO and functional groups of the textile.[36,43,44] The process of dipping and drying was repeated four times. The color of the textile changed from white color to brownish yellow color after immersing it in GO solution and drying in hot air oven as shown in Figure 1b. The brownish yellow colored textile is then chemically reduced in a solution of 5:1 (by volume ratio) acetic acid and hydriodic acid at 40 °C for 30 min that leads the textile color changed into black color as shown in Figure 1c. To remove the reaction solvents, RGT was washed with saturated sodium bicarbonate solution, DI water followed by methanol and then dried at 80 °C in hot air oven.

2.4. Fabrication of the RGT Strain Sensor

As prepared RGT was cut into 1.5 × 5cm and then electrical connections were made using copper tape attached with silver paste and epoxy glue to make firm connections.

2.5. Fabrication of RGT Electrodes Integrated Wearable Elastic Band for Electrophysiological Monitoring

As received iron-on adhesive and as fabricated RGT were cut into 3 × 3 cm square pieces and then placed on the wearable elastic band as shown in **Figure 2**a. After that, RGT was integrated with the wearable elastic band via iron-on adhesive by ironing as shown in Figure 2b. Finally, metal snap button was attached to interface with the Bio-Pac systems, Inc. (USA, MP36R) for electrophysiological signal acquisition as shown in Figure 2c. Figure 2d,e shows front and backside of the RGT electrode integrated wearable elastic band for electrophysiological signal monitoring while Figure 2f shows the enlarged view of the integrated RGT electrode along with snap button.

3. Characterization

The morphological studies were performed using Scanning Electron Microscope (Hitachi S3400N). Sheet resistance was measured by the Hall measurement system (HMS-3000). X-ray

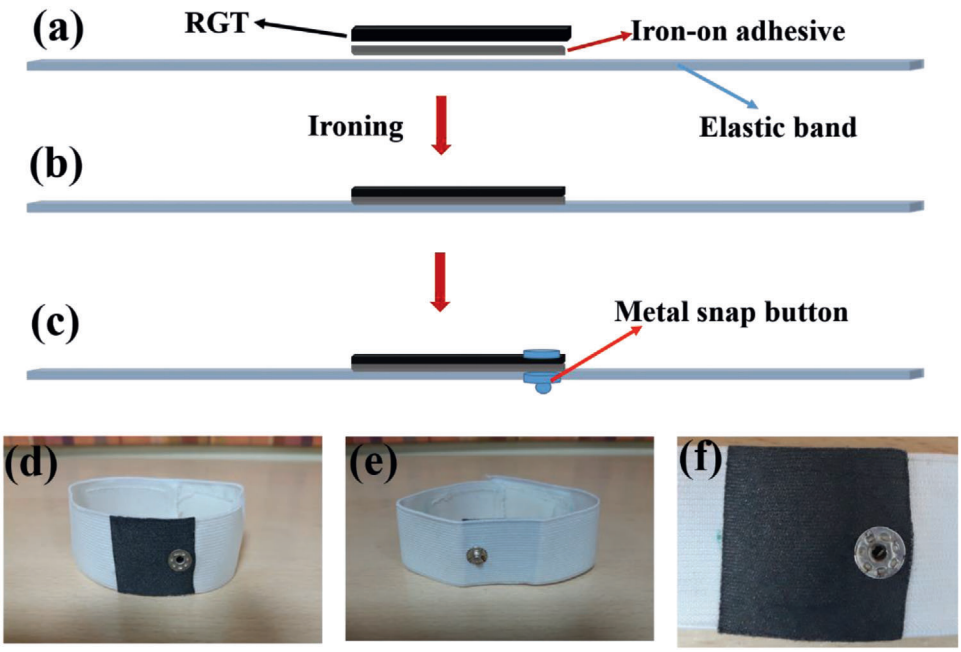

Figure 2. a–c) The fabrication of reduced graphene oxide (RGO) coated polyester knitted textile (RGT) electrodes integrated wearable elastic band for electrophysiological signal monitoring. d,e) Optical images of RGT electrodes integrated wearable elastic band for electrophysiological signal monitoring, and f) the enlarged view of integrated RGT electrode along with the snap button.

diffraction (XRD) was obtained by X' Pert Pro and EMPYREAN (PANalytical, The Netherlands) with a Cu K alpha (1.5406A°). Fourier transforms infrared (FTIR) spectra was obtained by the Jasco (FT/IR-6100) spectrometer. The electromechanical measurements were done by using a Precision Source/Meter Unit (Keysight-B2901A, Keysight Technologies-USA) and Mark 10 Force torque measurement Products (ESM 303, USA). Electrophysiological signals were monitored by using Biopac Systems, Inc. (USA, MP36R). The authors have involved and provided consent for all measurements.

4. Results and Discussions

4.1. Morphology and Wash Durability of the RGT

Figure 3a shows the amount of GO adsorbed onto the textile. The pristine textile was immersed in GO solution and then dried in a hot air oven. This process corresponds to one dip and dry cycle. The above process was repeated four times and the amount of adsorbed GO was calculated. As shown in Figure 3a, the amount of adsorbed GO (wt%) increases with number of dipping cycles. After that, GO coated textile was chemically reduced to obtain RGO coated textile (RGT). The sheet resistance (R_s) of as prepared RGT textile was calculated to be 0.23 KΩ sq^{-1}. The wash durability is vital for the textile coated with conductive materials for their stability, reliability, and re-usability. We further performed wash durability of the RGT to observe adhesion between RGO nanosheets and textiles. In order to test this, the RGT was immersed in 500 mL beaker containing soap water (5 g L^{-1}) and, then continuously stirred at 1000 rpm for 5 min. This process is considered as one washing cycle. Figure 3b shows the sheet resistance of the RGT versus number of washing cycles. The sheet resistance of the RGT after first and fifth washing cycle was calculated to be 0.26 and 0.32 KΩ sq^{-1}, respectively, and the RGT sheet resistance increased by approximately 39% after five washing cycles (Figure S2, Supporting Information), indicating its good wash durability because of van der Waals interaction between the RGO nanosheets and surface of the textile (see Movie S1, Supporting Information).[23,36] Figure S3 (Supporting Information) presents the XRD pattern of GO, GO coated polyester knitted textile, and RGT. A characteristic diffraction peak of GO is observed at 2θ angles of 10.01° with an interlayer spacing of about 0.88 nm.[45] GO coated polyester knitted textile showed the three prominent diffraction peaks of polyester textile at 2θ angles of 17.3°, 22.6°, and 25.5° along with GO diffraction peak, revealing the deposition of GO on the textile. After reducing GO to RGO, the GO diffraction peak moves to higher angles and merges with textile peaks.[46] Figure S4 (Supporting Information) shows the FTIR spectra of polyester knitted textile, GO coated polyester knitted textile, and RGT. As shown in Figure S4 (Supporting Information), polyester textile revealed characteristic peaks, which are observed at 718 cm^{-1} (to out of plane benzene group), 1014 cm^{-1} (in plane vibration of benzene), 1084 and 1235 cm^{-1} (ester C=O stretching), and 1718 cm^{-1} (CO groups of aromatic ester).[47] In addition to the polyester peaks, polyester knitted textile coated with GO showed the peaks at 1261 and 1728 cm^{-1} assigned to C=O and C−O stretching vibration of GO while these peaks intensities decreased in the RGT, confirming the presence of GO and RGO on the textile.[45] Figure 3c–e shows the SEM images of the pristine textile at different magnifications. Figure 3c reveals interlocked knitted textile, made with continuous polyester filament yarn. As shown in Figure 3d,e, polyester yarn is composed of smooth twisted fibers with the average diameter of 15 µm. Figure 3f–h shows SEM image of the RGO coated textile at different

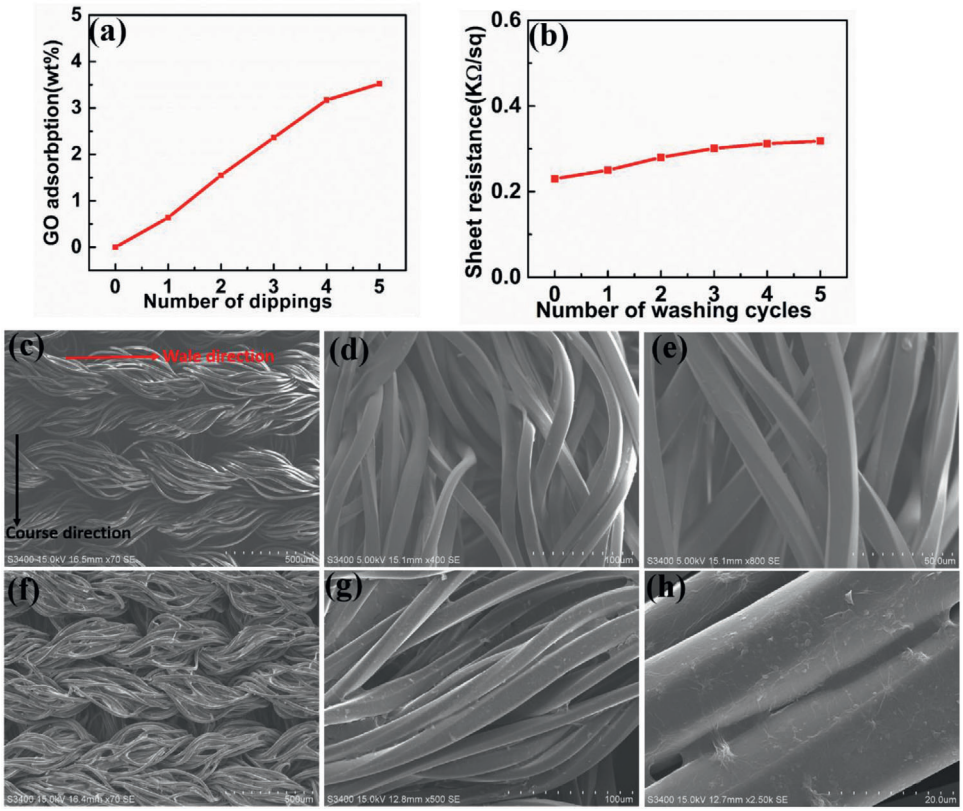

Figure 3. a) Amount of graphene oxide (GO) adsorbed onto the textile with the number of dippings, b) sheet resistance of RGO coated polyester knitted textile (RGT) versus number of washing cycles, c–e,f–h) SEM images of the pristine textile and RGT, respectively, at different magnifications.

magnification. Figure 3f discloses uniform coating of RGO on pristine textiles. As shown in Figure 3g,h, RGO coated fibers in the yarn were connected to one another via RGO (Figure S5, Supporting Information).

4.2. Electromechanical Behavior of the RGT Strain Sensor

In order to study the electromechanical behavior of the RGT, the RGT was cut into 5 cm length along the course and wale direction with width of 1.5 cm and then electrical connections were made to obtain RGT strain sensor in both course and wale direction as shown in **Figure 4**a. Before performing the electromechanical measurements, the RGT strain sensors signal is stabilized by applying random cyclic strain along the course and wale direction. During this process, possible structural damages (cracking or peeling off) caused to deposited RGO on the textile, thus reducing further damages while performing electromechanical measurements. Figure S6a,b (Supporting Information) present SEM images of the RGT strain sensor at a different magnification after repeated stretching and releasing (Figure S6, Supporting Information). As shown in Figure S6a,b (Supporting Information), possible cracks in the deposited RGO on the textile can be observed. Figure 4b,c shows the relative change in resistance (RCR) as a function of strain for the RGT strain sensor along the course and wale direction, respectively. The negative RCR indicates that the decrease in resistance of the RGT strain sensor with an increasing strain along the course and wale direction. The gauge factor (GF) or sensitivity of a strain sensor is defined as slope of the RCR versus strain curve, which is given by

$$GF = \delta(\Delta R/R_0\%)/\delta\varepsilon \quad (1)$$

where $\Delta R = (R_\varepsilon - R_0)$, R_0 and R_ε are the resistance of a sensor under zero strain and applied strain, and ϵ is the applied strain. GF of the RGT strain sensor is calculated to be 4.1 and 8 at a strain of 5% along the course and wale direction, which are higher than the metal strain gauges and comparable that of the recently reported graphene coated textile strain sensors.[36,38,48,49] Sensitivity or GF of metal strain gauges is given by $(GF) = (\Delta R/R)/\epsilon = (1 + 2\nu) + (\Delta\rho/\rho)/\epsilon$, where ν is the Poisson's ratio (ν = 0.2–0.5 for most of the metals), ϵ applied strain and ρ is the resistivity of metal. In metals, resistivity is constant, and sensitivity depends on the Poisson's ratio (ν). Most of the metal strain gauges exhibit low sensitivity (GF = 1.6–2).[48]

The electrical properties of knitted textiles depend on the number of fiber/yarns contacts points and contact pressure between the adjacent conductive loops. According to Holms Theory, the contact resistance between the two conductive parts of textile is given by

$$X_c = \left[\frac{\Delta H_m}{\Delta H_m^0} \cdot w\right] * 100 \quad (2)$$

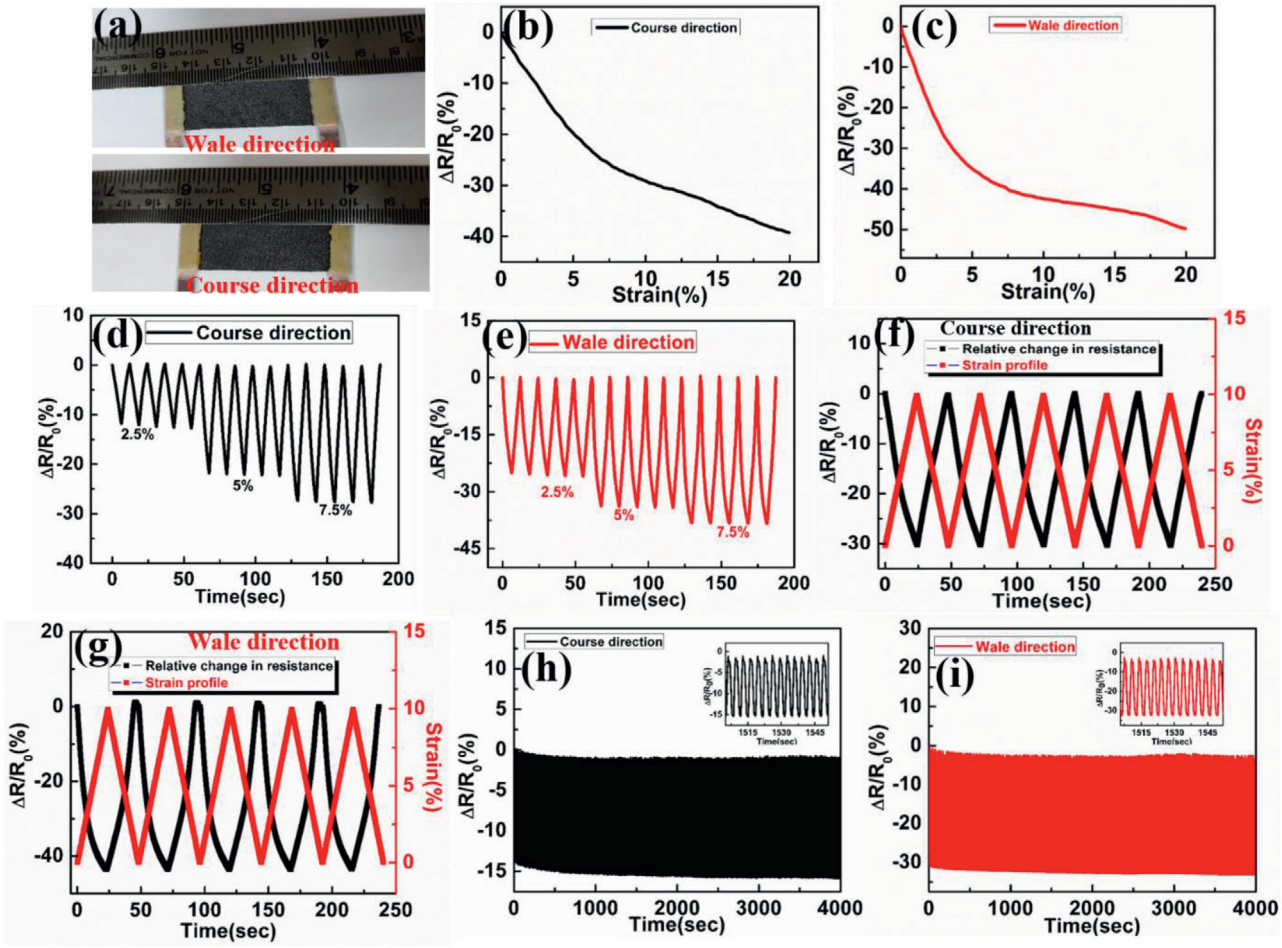

Figure 4. Electromechanical performance of the reduced graphene oxide (RGO) coated polyester knitted textile (RGT) strain sensor a) optical images of the RGT strain sensor along the course and wale direction, b,c) strain-dependent relative change in resistance (RCR) of a sensor along the course and wale direction, respectively. d,e) Cyclic loading and unloading of a sensor at different strains of 2.5%, 5%, and 7.5% at a strain frequency of 0.08 Hz along the course and wale direction, respectively, f,g) RCR (black) response of a sensor to cyclic strain (red) of 10% along the course and wale direction, respectively, and h,i) stability and durability of a sensor under cyclic loading and unloading of strain 3% for 1500 cycles along the course and wale direction respectively.

where the R_C is the contact resistance, ρ is the resistivity of fiber/yarns, H is materials hardness, n is the number of contact points among the conductive yarns/twisted fibers and P is the contact pressure.[50] When the knitted textile is subjected to external strain along the course and wale direction, the loop configuration of the knitted structure will change rather than an increase in the length of the yarn in the structure as shown in Figure S7 (Supporting Information). Moreover, twisted fibers in the yarn become more and more close. According to contact resistance theory, contact resistance between the two conductive parts of textiles decreases when the number of contact points and the contact pressure increase. When the RGT strain sensor is stretched, increase in the contact pressure and number of contact points among the fibers within the yarn and the adjacent conductive loops of yarn in the textile leads to decrease in the resistance of the RGT strain sensor along the stretching direction. As shown in Figure S7 (Supporting Information), decrease in the resistance of the textile is more in the wale direction when compared with the course direction due to more and more number of contact points and high contact area among the fibers within the yarn and adjacent conductive loops of yarns at a particular strain, resulting into high sensitivity along the wale direction. Figure S8a,b (Supporting Information) shows the RGT strain sensor response to a small strains along the course and wale direction (Figure S8, Supporting Information). As shown in Figure S8a,b (Supporting Information), the RGT strain sensor could detect the strains as small as 0.1% along the course and the wale direction.

Figure 4d,e shows the RCR of a strain sensor versus time under cyclic stretching and releasing at a strain of 2.5%, 5%, and 7.5% along the course and wale direction, respectively. As shown in Figure 4d,e, the RCR decreases with increasing the applied strain, these results are similar to the results shown in Figure 4b,c, respectively. Figure 4f,g reveals the RCR response of the RGT strain sensor to cyclic loading and unloading for 10% strain along the course and wale direction. As shown in Figure 4f,g, the RGT sensor exhibits initial resistance under zero strain while sensor exhibits lower resistance at a strain of 10%, indicating good response and excellent synchronization with the

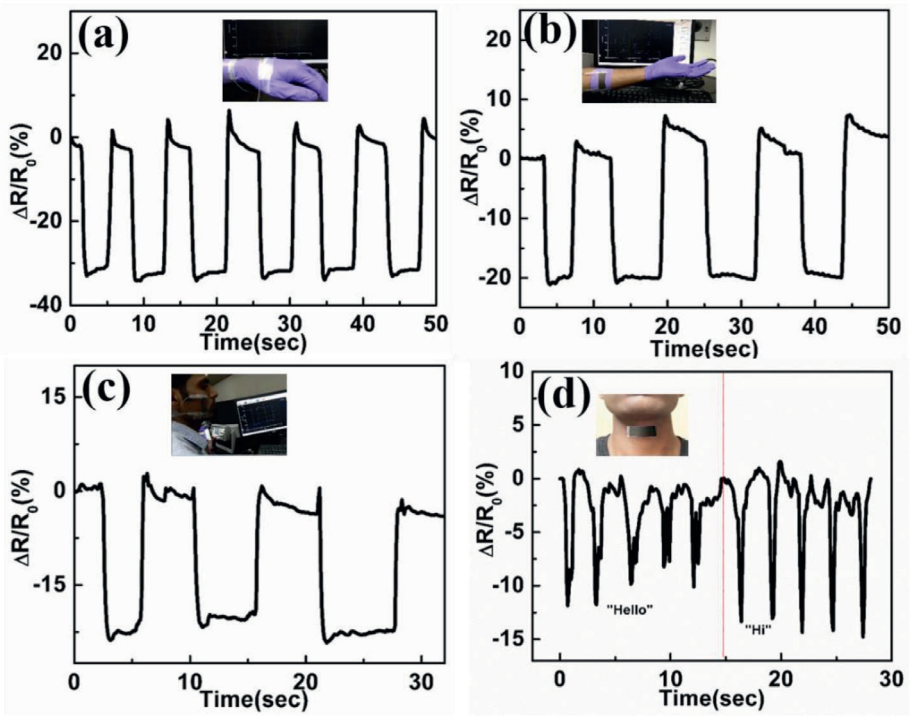

Figure 5. Human motion detection using the reduced graphene oxide (RGO) coated polyester knitted textile (RGT) strain sensor. The sensor response to a) wrist bending and straightening, b) forearm muscle movement, c) cheek bulging and relaxing, and d) throat muscle movement associated with phonation such as "Hello" and "Hi."

applied strain. Figure S9a,b (Supporting Information) shows the hysteresis behavior of the RGT strain sensor under loading and unloading for 10% strain along the course and wale direction, respectively (Figure S9, Supporting Information). As shown in Figure S9a,b (Supporting Information), the RGT strain sensor exhibits hysteresis along both directions of stretching, which may be attributed to the recovery and relaxation of fabric with time during unloading.[42,51] In order to study the effect of strain frequency on the RCR of the RGT strain sensor, sensor was subjected to cyclic stretching and releasing at a strain of 5% along both directions. As shown in Figure S10a,b (Supporting Information), it can be observed that the peak value of the RCR is the same irrespective of strain frequency within the measured strain frequency range of 0.1 to 0.4 Hz. Figure 4h,i shows the stability and durability of the RGT strain sensor upon cyclic loading and unloading at a strain 3% for more than 1500 cycles. Figure S11a, b (Supporting Information) reveals the response and recovery time of the RGT strain sensor along the course and the wale direction under a strain of 2% (Figure S11, Supporting Information). As shown in Figure S11a,b (Supporting Information), the response and recovery time of the RGT strain sensor along the course direction are about 80 and 100 ms, while along the wale direction, about 90 and 110 ms, respectively.

4.3. Application of the RGT Strain Sensor in Human Motion Detection

Due to its excellent stability, reliability, high sensitivity and wash durability, the RGT strain sensor exhibits potential applications in real-time human motion detection. **Figure 5**a–d shows human motion tracking by using the RGT strain sensor. RGT strain sensor detects and monitors the wrist joint bending and straightening as shown in Figure 5a. As shown in Figure 5b, forearm muscle movements generated by open hand and clenched fist could be monitored by the RGT strain sensor (see Movie S2, Supporting Information). Figure 5c shows the response of the RGT strain sensor to cheek bulging and relaxing, revealing that sensor could be used to monitor the facial expression. As shown in Figure 5d, the sensor was mounted on the throat in order to track throat movements associated with the phonation such as "Hello" and "Hi." As shown in Figure 5d, distinct and repeatable RCR patterns were observed when the subject spoke "Hello" and "Hi."

4.4. Electrophysiological Signal Monitoring by Using RGT Electrodes Integrated Wearable Elastic Band

All electrophysiological signals were measured using a 4-channel acquisition system with a notch filter (50 Hz cut-off frequency) (Bio-Pac systems, Inc., USA, MP36R) to remove the power line noise. When the subject wore the RGT electrodes integrated wearable elastic bands on the chest and abdomen, the RGT electrodes were positioned on left and right chest, and left and right abdomen parts, respectively, as shown in **Figure 6**a. The left arm and right arm are replaced by left and right chest, respectively, while the left and right legs are replaced by left and right abdomen parts, respectively. The conventional Ag/AgCl electrodes were also mounted on the subject adjacent to the RGT electrodes to compare the obtained ECG signals from both the electrodes.

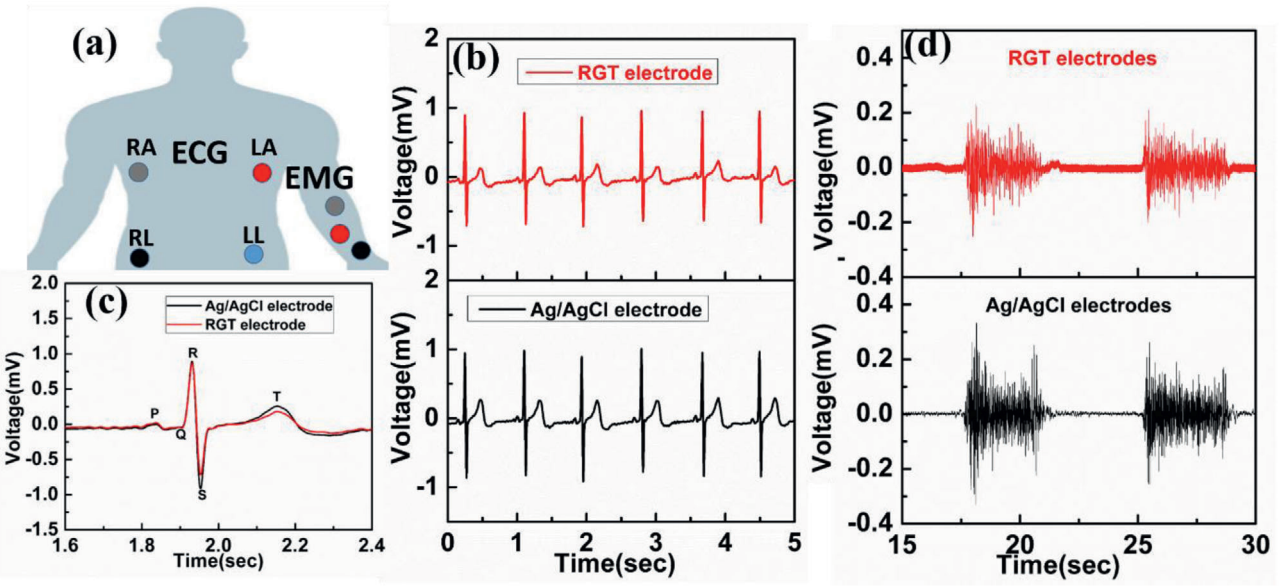

Figure 6. a) The conventional Ag/AgCl and reduced graphene oxide (RGO) coated polyester knitted textile (RGT) electrode placement for measuring electrophysiological signals (right arm (RA), left arm (LA), right leg (RL), left leg (LL), gray, red, and black dots on the hand represent positive, negative, and ground electrode, respectively). b) Recorded ECG signals from Ag/AgCl and RGT electrodes, c) various ECG signal features d) acquired EMG signals from Ag/AgCl and RGT electrodes.

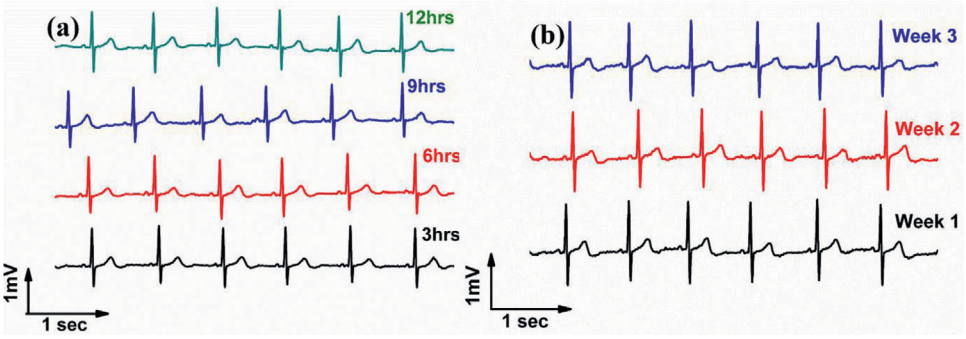

Figure 7. a) Continuous and long-term ECG signals measured from the reduced graphene oxide (RGO) coated polyester knitted textile (RGT) electrodes for every 3 h when wearing continuously for a period of 12 h and (b) re-usability of the RGT electrodes. Recorded ECG signals for weeks 1, 2, and 3, respectively.

The ECG signals were simultaneously measured from both the conventional Ag/AgCl and RGT electrodes as shown in 6b. As shown in Figure 6b, similar type of ECG waveforms were observed from both the electrodes. Figure 6c shows enlarged view of ECG signals and it can be observed that various features of ECG signal such as P wave, QRS complex, and T wave are clearly distinguished for both the electrodes, which can provide valuable medical information about functioning of the heart.

The signal to noise ratios (SNR) of the conventional Ag/AgCl and RGT electrodes were calculated to be 25 and 23.45 dB, respectively. To measure the electromyography (EMG) signals, the RGT electrodes integrated wearable elastic band was mounted on the forearm along with conventional Ag/AgCl electrodes as shown in Figure 6a. The gray, red, and black dots on the hand are the positive, negative, and ground electrodes, respectively, for EMG signal acquisition. The EMG signals obtained from the RGT electrodes were similar to that of the conventional Ag/AgCl electrodes as shown in Figure 6d. In order to obtain three limb leads (Lead I, Lead II, and Lead III) and three augmented leads (aVR, aVL, and aVF), four electrodes are required and their placements on human body are shown in Figure 6a. Lead I and Lead II ECG signals were obtained from the Bio-Pac systems, Inc. (USA, MP36R) and rest of the Limb lead (i.e., Lead III) is calculated from acquired Lead I and II, and augmented Leads were calculated in real-time from three limb leads by using Biopac Student Lab 4.1 software. Figure S12 (Supporting Information) shows the six Lead ECG signals measured from RGT electrodes.

We further demonstrated the continuous and long-term monitoring of the ECG signals and also re-usability of the RGT electrodes. The RGT electrodes integrated wearable elastic bands were worn continuously for the period of 12 h as shown in Figure 6a and the ECG signals were obtained every 3 h. **Figure 7**a shows the acquired ECG signals from the RGT electrodes for 3, 6, 9, and 12h. It can be seen from Figure 7a that, similar ECG

signals were observed on continuously wearing the RGT electrodes at 3 and 12 h, showing their ability to monitor continuous and long-term ECG signals.

In order to demonstrate the reusability of the RGT electrodes, ECG signals were measured for weeks 1, 2, and 3. Figure 7b illustrates the acquired ECG signals from the RGT electrodes for weeks 1, 2, and 3. The RGT electrodes integrated wearable elastic band was cleaned with water and then dried at ambient condition before measuring ECG signal for every week. As shown in Figure 7b, no significant variations in ECG signals were observed even after 3 weeks, which indicates the possibility of multiple usages of the RGT electrodes. Based on the above results, i.e., wearable comfort of RGT, wash durability, biocompatible nature[52] of coated RGO on textile, and novel approach to integrate with wearable elastic band, one can strongly suggest that fabricated RGT electrodes can be employed for continuous and long-term monitoring of electrophysiological signals and can be re-used for several times.

5. Conclusions

In conclusion, we fabricated multifunctional, wash durable, reusable, and highly conductive RGT by dip-dry-reduce method. The sheet resistance of the RGT textile was measured to 0.23 KΩ sq^{-1} and its sheet resistance increased to 0.32 KΩ sq^{-1} after five washing cycles, indicating its excellent wash durability. The RGT as a strain sensor exhibited GF of 4.1 and 8 at a strain of 5% along the course and wale direction, respectively, which are comparable to those of the reported textile strain sensors. The RGT strain sensor showed stability and durability for cyclic loading and unloading and outstanding performance in monitoring human motion. Further, RGT as an electrode integrated to the wearable elastic band for electrophysiological signal monitoring. The electrophysiological signals obtained from both the conventional Ag/AgCl electrodes and RGT electrodes are comparable and SNR of acquired ECG signal from both electrodes are 25 and 23.45 dB, respectively. To demonstrate continuous and long-term signal monitoring, the RGT electrodes integrated wearable elastic band wore continuously for 12 h and similar ECG signals were obtained for every 3 h. The RGT electrodes can be used for several times after washing, indicating re-usability, and reliability.

Supporting Information

Supporting Information is available from the Wiley Online Library or from the author.

Acknowledgements

This research work was supported by the Department of Science and Technology (DST) and Indian Space Research Organization (ISRO), India (Grant Nos. RD/0119-ISROC00-018). The authors acknowledge the Centre for Excellence in Nanoelectronics (CEN), Sophisticated Analytical Instrument Facility (SAIF) and Department of Metallurgical Engineering and Materials Science (MEMS) at the Indian Institute of Technology Bombay (IIT Bombay), Mumbai, for providing various facilities for fabrication and characterization of the device.

Conflict of Interest

The authors declare no conflict of interest.

Data Availability Statement

Research data are not shared.

Keywords

conductive fabrics, electrophysiological signals, multifunctional, reduced graphene oxide, wash durable

Received: December 23, 2020
Revised: January 11, 2021
Published online:

[1] G. Schwartz, B. C. K. Tee, J. Mei, A. L. Appleton, D. H. Kim, H. Wang, Z. Bao, *Nat. Commun.* **2013**, *4*, 1858.
[2] H. Jin, Y. S. Abu-Raya, H. Haick, *Adv. Healthcare Mater.* **2017**, *6*, 1700024.
[3] H. H. Chou, A. Nguyen, A. Chortos, J. W. F. To, C. Lu, J. Mei, T. Kurosawa, W. G. Bae, J. B. H. Tok, Z. Bao, *Nat. Commun.* **2015**, *6*, 8011.
[4] D. Y. Park, D. J. Joe, D. H. Kim, H. Park, J. H. Han, C. K. Jeong, H. Park, J. G. Park, B. Joung, K. J. Lee, *Adv. Mater.* **2017**, *29*, 1702308.
[5] T. Yang, X. Jiang, Y. Zhong, X. Zhao, S. Lin, J. Li, X. Li, J. Xu, Z. Li, H. Zhu, *ACS Sens.* **2017**, *2*, 967.
[6] S. Kim, S. Oh, Y. Jung, H. Moon, H. Lim, *ACS Omega* **2018**, *3*, 1110.
[7] S. J. Park, J. Kim, M. Chu, M. Khine, *Adv. Mater. Technol.* **2018**, *3*, 1700158.
[8] Y. Yang, N. Sun, Z. Wen, P. Cheng, H. Zheng, H. Shao, Y. Xia, C. Chen, H. Lan, X. Xie, C. Zhou, J. Zhong, X. Sun, S. T. Lee, *ACS Nano* **2018**, *12*, 2027.
[9] Y. Zhou, X. Wang, L. Acauan, E. Kalfon-Cohen, X. Ni, Y. Stein, K. K. Gleason, B. L. Wardle, *Adv. Mater.* **2019**, *31*, 1901916.
[10] Y. Liu, J. J. S. Norton, R. Qazi, Z. Zou, K. R. Ammann, H. Liu, L. Yan, P. L. Tran, K. I. Jang, J. W. Lee, D. Zhang, K. A. Kilian, S. H. Jung, T. Bretl, J. Xiao, M. J. Slepian, Y. Huang, J. W. Jeong, J. A. Rogers, *Sci. Adv.* **2016**, *2*, 1601185.
[11] M. Amjadi, K. U. Kyung, I. Park, M. Sitti, *Adv. Funct. Mater.* **2016**, *26*, 1678.
[12] Y. Zang, F. Zhang, C. A. Di, D. Zhu, *Mater. Horiz.* **2015**, *2*, 140.
[13] R. R. Kisannagar, P. Jha, A. Navalkar, S. K. Maji, D. Gupta, *ACS Omega* **2020**, *5*, 10260.
[14] H. Lee, D. Kwon, H. Cho, I. Park, J. Kim, *Sci. Rep.* **2017**, *7*, 39837.
[15] T. Kim, J. Park, J. Sohn, D. Cho, S. Jeon, *ACS Nano* **2016**, *10*, 4770.
[16] B. You, C. J. Han, Y. Kim, B. K. Ju, J. W. Kim, *J. Mater. Chem. A* **2016**, *4*, 10435.
[17] S. Gong, D. T. H. Lai, B. Su, K. J. Si, Z. Ma, L. W. Yap, P. Guo, W. Cheng, *Adv. Electron. Mater.* **2015**, *1*, 1400063.
[18] X. Fan, W. Nie, H. Tsai, N. Wang, H. Huang, Y. Cheng, R. Wen, L. Ma, F. Yan, Y. Xia, *Adv. Sci.* **2019**, *6*, 1900813.
[19] J. Chen, J. Liu, T. Thundat, H. Zeng, *ACS Appl. Mater. Interfaces* **2019**, *11*, 18720.
[20] X. Fu, T. Li, F. Qi, S. Zhang, J. Wen, W. Shu, P. Luo, R. Zhang, S. Hu, Q. Liu, *Appl. Surf. Sci.* **2020**, *507*, 145135.
[21] E. N. Zare, P. Makvandi, B. Ashtari, F. Rossi, A. Motahari, G. Perale, *J. Med. Chem.* **2020**, *63*, 1.
[22] W. Weng, P. Chen, S. He, X. Sun, H. Peng, *Angew. Chem., Int. Ed.* **2016**, *55*, 6140.
[23] S. Qiang, T. Carey, A. Arbab, W. Song, C. Wang, F. Torrisi, *Nanoscale* **2019**, *11*, 9912.
[24] J. Xiong, P. Cui, X. Chen, J. Wang, K. Parida, M. F. Lin, P. S. Lee, *Nat. Commun.* **2018**, *9*, 4280.
[25] S. H. Ha, K. H. Shin, H. W. Park, Y. J. Lee, *Small* **2018**, *14*, 1703418.

[26] M. K. Yapici, T. Alkhidir, Y. A. Samad, K. Liao, *Sens. Actuators, B* **2015**, *221*, 1469.
[27] L. Wang, X. Fu, J. He, X. Shi, T. Chen, P. Chen, B. Wang, H. Peng, *Adv. Mater.* **2020**, *32*, 1901971.
[28] M. K. Yapici, T. E. Alkhidir, *Sensors* **2017**, *17*, 875.
[29] S. J. Kim, W. Song, Y. Yi, B. K. Min, S. Mondal, K. S. An, C. G. Choi, *ACS Appl. Mater. Interfaces* **2018**, *10*, 3921.
[30] K. Arquilla, A. K. Webb, A. P. Anderson, *Sensors* **2020**, *20*, 1013.
[31] Y. Wei, S. Chen, Y. Lin, X. Yuan, L. Liu, *J. Mater. Chem. C* **2016**, *4*, 935.
[32] Z. Yang, Y. Pang, X. L. Han, Y. Yang, Y. Yang, J. Ling, M. Jian, Y. Zhang, T. L. Ren, *ACS Nano* **2018**, *12*, 9134.
[33] N. Karim, S. Afroj, S. Tan, P. He, A. Fernando, C. Carr, K. S. Novoselov, *ACS Nano* **2017**, *11*, 12266.
[34] H. Wang, H. Wang, Y. Wang, X. Su, C. Wang, M. Zhang, M. Jian, K. Xia, X. Liang, H. Lu, S. Li, Y. Zhang, *ACS Nano* **2020**, *14*, 3219.
[35] M. Yang, J. Pan, A. Xu, L. Luo, D. Cheng, G. Cai, J. Wang, B. Tang, X. Wang, *Polymers* **2018**, *10*, 23.
[36] D. Du, P. Li, J. Ouyang, *J. Mater. Chem. C* **2016**, *4*, 3224.
[37] N. Luo, W. Dai, C. Li, Z. Zhou, L. Lu, C. C. Y. Poon, S. C. Chen, Y. Zhang, N. Zhao, *Adv. Funct. Mater.* **2016**, *26*, 1178.
[38] J. J. Park, W. J. Hyun, S. C. Mun, Y. T. Park, O. O. Park, *ACS Appl. Mater. Interfaces* **2015**, *7*, 6317.
[39] J. V. Lidón-Roger, G. Prats-Boluda, Y. Ye-Lin, J. Garcia-Casado, E. Garcia-Breijo, *Sensors* **2018**, *18*, 300.
[40] A. Ankhili, X. Tao, C. Cochrane, D. Coulon, V. Koncar, *Materials* **2018**, *11*, 256.
[41] K. Dong, X. Peng, Z. L. Wang, *Adv. Mater.* **2019**, *32*, 1902549.
[42] R. Reddy K, S. Gandla, D. Gupta, *Adv. Mater. Interfaces* **2019**, *6*, 1900409.
[43] D. Konahge, J. Foroughi, S. Gambhir, G. M. Spinks, G. G. Wallace, *RSC Adv.* **2016**, *6*, 73203.
[44] J. Molina, J. Fernández, J. C. Inés, A. I. Del Río, J. Bonastre, F. Cases, *Electrochim. Acta* **2013**, *93*, 44.
[45] D. C. Marcano, D. V. Kosynkin, J. M. Berlin, A. Sinitskii, Z. Sun, A. Slesarev, L. B. Alemany, W. Lu, J. M. Tour, *ACS Nano* **2010**, *4*, 4806.
[46] V. Babaahmadi, M. Montazer, W. Gao, *Carbon* **2017**, *118*, 443.
[47] J. M. Andanson, S. G. Kazarian, *Macromol. Symp.* **2008**, *265*, 195.
[48] G. R. Higson, *J. Sci. Instrum.* **1964**, *41*, 405.
[49] H. Lee, M. J. Glasper, X. Li, J. A. Nychka, J. Batcheller, H. J. Chung, Y. Chen, *J. Mater. Sci.* **2018**, *53*, 9026.
[50] R. Holm, *Electric Contacts: Theory and Application*, Springer, Berlin **2010**.
[51] O. Atalay, W. Richard Kennon, M. Dawood Husain, *Sensors* **2013**, *13*, 11114.
[52] J. Kim, *Int. J. Nanomed.* **2016**, *11*, 1927.